Analytical and numerical tools for vacuum systems

R. Kersevan
ESRF, Grenoble, France

Abstract
Modern particle accelerators have reached a level of sophistication which require a thorough analysis of all their sub-systems. Among the latter, the vacuum system is often a major contributor to the operating performance of a particle accelerator. The vacuum engineer has nowadays a large choice of computational schemes and tools for the correct analysis, design, and engineering of the vacuum system. This paper is a review of the different type of algorithms and methodologies which have been developed and employed in the field since the birth of vacuum technology. The different level of detail between simple back-of-the-envelope calculations and more complex numerical analysis is discussed by means of comparisons. The domain of applicability of each method is discussed, together with its pros and cons.

1 Introduction

The vast majority of particle accelerators need low pressures in order to work efficiently and reduce beam losses and radiation background. Therefore in the following only the case of molecular flow conditions will be considered, i.e., when the interaction of residual gas molecules with each other is negligible, and the molecules are supposed to be hitting only the walls of the vacuum chamber. We will refer often in the following to this situation as 'UHV conditions'.

In general, for the calculation of pressure profiles and conductances, two different approaches are possible: analytical methods and numerical methods. The former are appealing, as they allow the calculation using formulae, a solution which eases the exploration of the space of different configurations of the vacuum system under study. For example, one could implement one or more formulae into a spreadsheet and then change some parameters such as the spacing of the pumps, their size, or the geometry of the chamber, until the specified design performance is reached. Unfortunately, there are no universal formulae which could be used. Only very simple geometries can be tackled analytically in a correct way, but a real life accelerator often departs from this case.

The other approach, employing numerical methods, is more widespread, although this often makes use of existing formulae, derived analytically. One variant of the numerical approach, the Monte Carlo (MC) method, directly implements the formulae of the kinetic theory of gases, with no simplifications. Its major drawback is that it is CPU-intensive.

With few exceptions, the vacuum systems of particle accelerators fall under the category of conductance limited systems. In order to clarify what this means, the basic concept of conductance is revisited, using both analytic tools and numerical ones.

We then move on to review the different ways of solving the basic equations, mass-flow balance equations, which describe the behaviour of gases inside a vacuum system. Different ways of solving such equations are given, with particular emphasis on their applicability.

A rather large body of literature has been used to cover all possible aspects of the subject. Several references are given throughout the text: they should be consulted carefully and critically and used as a guidance for the implementation of vacuum calculations.

2   Conductance calculations

Much has been written concerning the concept of conductance [1–3]. Alongside with the basic equation of UHV technology

$$P = \frac{Q}{S} \tag{1}$$

it is one of the primary concepts through which many other interesting quantities can be calculated, such as the effective pumping speed and the average pressure.

Conductance is defined as the ratio of throughput to pressure differential, under steady conditions, where the pressures refer to two isobaric sections inside the pumping system, as indicated in Fig. 1.
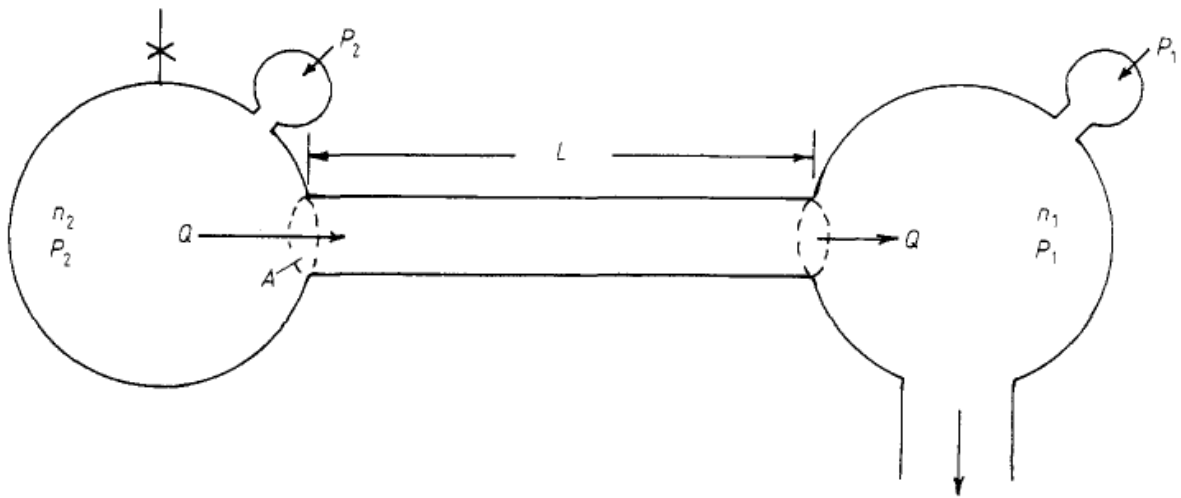

Fig. 1: Experimental set-up for the measurement of the flow resistance (conductance) of a tube [4]

In a less rigorous way, the conductance of a vacuum component is its capacity to let a volume of gas pass from one end to the other, regardless of the pressure differential. It is, basically, a function of the geometry of the system.

2.1   Analytic calculations

In one of the fundamental papers of vacuum technology [1], Knudsen wrote that the 'flow resistance' Z (1/conductance) of a tube of length L, cross-sectional area A, and perimeter S is given by

$$Z = \frac{3}{8}\sqrt{\pi/2}\int_0^L \frac{S}{A^2}\,\mathrm{d}l \quad . \tag{2}$$

Smoluchovski and Clausing [2,3] realized that Knudsen's formula was correct only in the particular case of a circular cross-section. In all other cases a correction factor had to be introduced, and the simple integral in Eq. (2) changed to the double integral

$$I = \int_S \int_{-\pi/2}^{\pi/2} \frac{1}{2}\rho^2 \cos\theta\,\mathrm{d}\theta\,\mathrm{d}s \quad . \tag{3}$$

Figure 2 (a) and 2 (b) show the definition of the variables.
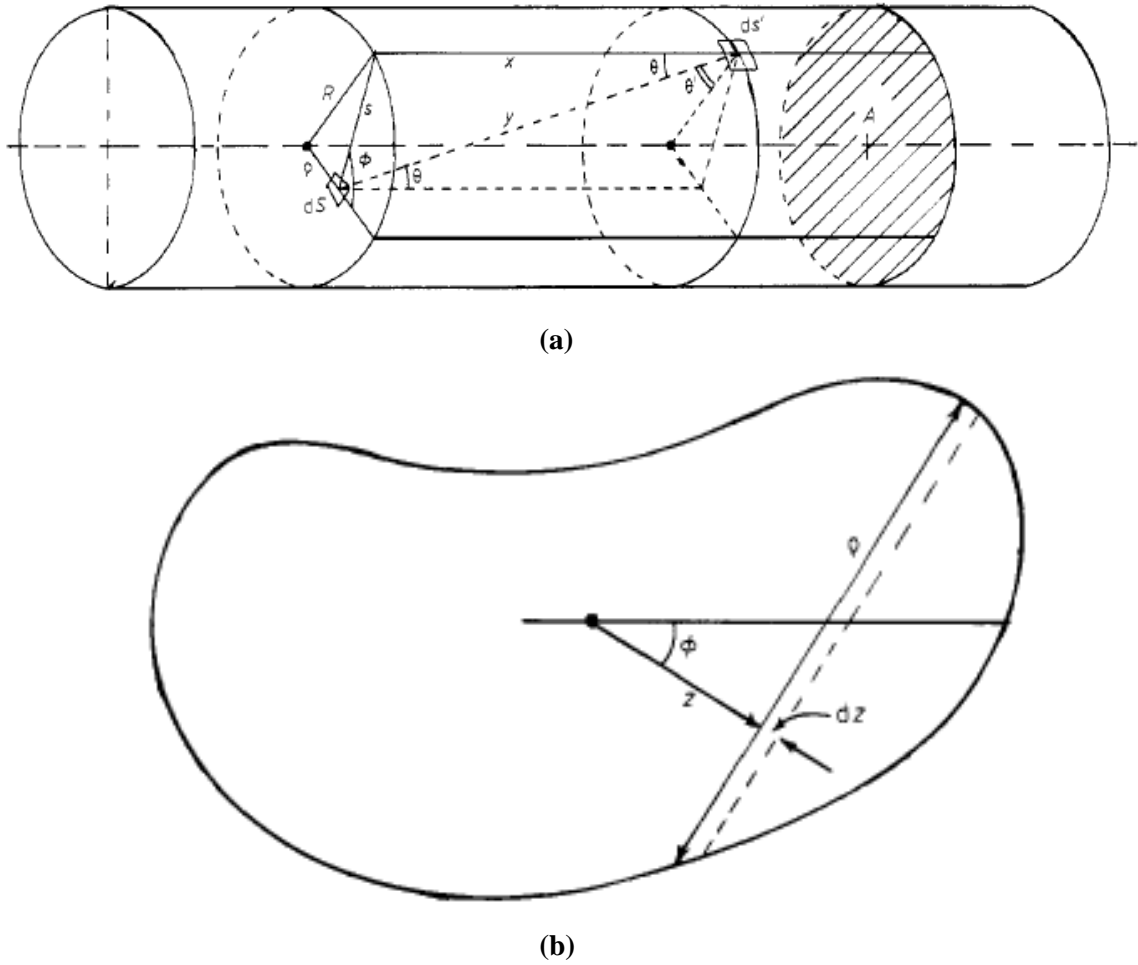
(a)

(b)

Fig. 2: (a), (b) Definition of variables for the calculation of Smoluchovski's integral [4]

It was shown later that the double integral above can be replaced by [4]

$$I = \pi \cdot \text{avg}\left(\int \rho^2 \, \mathrm{d}z\right) \ . \tag{4}$$

As already pointed out by Clausing [2], for a tube of arbitrary shape it is better to use the concept of transmission probability $P_{i \to j}$, i.e., the ratio of the molecules which reach the 'exit' j of the tube once they are injected through its 'entrance' i (whether or not i and j are the real entrance and exit of the tube). The relationship between the conductance C in litre $\cdot$ s^{-1} and $P_{i \to j}$ is given by (Ref. [5], p. 86)

$$C = \frac{\overline{v}}{4} \cdot A \cdot P_{i \to j} \ . \tag{5}$$

where A is the entrance area in cm^2, and $\overline{v}$ is the average molecular speed in m $\cdot$ s^{-1} given by

$$\overline{v} = \sqrt{\frac{8kT}{\pi m}} = \sqrt{\frac{8RT}{\pi M}} \tag{6}$$

with k = Boltzmann's constant ($k = 1.381 \cdot 10^{-23}$ J $\cdot$ K^{-1}); m = molecular mass (kg); $R = 8.314$ J $\cdot$ mole^{-1}; M = molar weight (kg $\cdot$ mole^{-1}).

The resolution of Eq. (3) becomes difficult as soon as the cross-section of the tube is not as simple as a circle, ellipse or rectangle. A typical vacuum system of an accelerator is a sequence of tubes with different cross-sections, connected together. In this case it would be tempting to think of the total conductance of the system as the one obtained using an electrical circuit analogy of the flow resistance mentioned above Z_{tot}, where the resistance of each section of the tube having a given cross-section is calculated separately assuming that it connects two separate volumes as shown in Fig. 1, and then the reciprocal of these are summed up in order to obtain $1/Z_{tot}$ (Ref. [5], p. 96). This procedure would generate the wrong result, as it would not take into account the so-called beaming effect [2–4], which describes the fact that while the molecules move along the tube from the entrance to the exit, their average velocity vectors become more and more parallel to the axis of the tube. This had been recognized early on by Clausing [2], and re-visited later by several authors [4], as shown in Fig. 3.
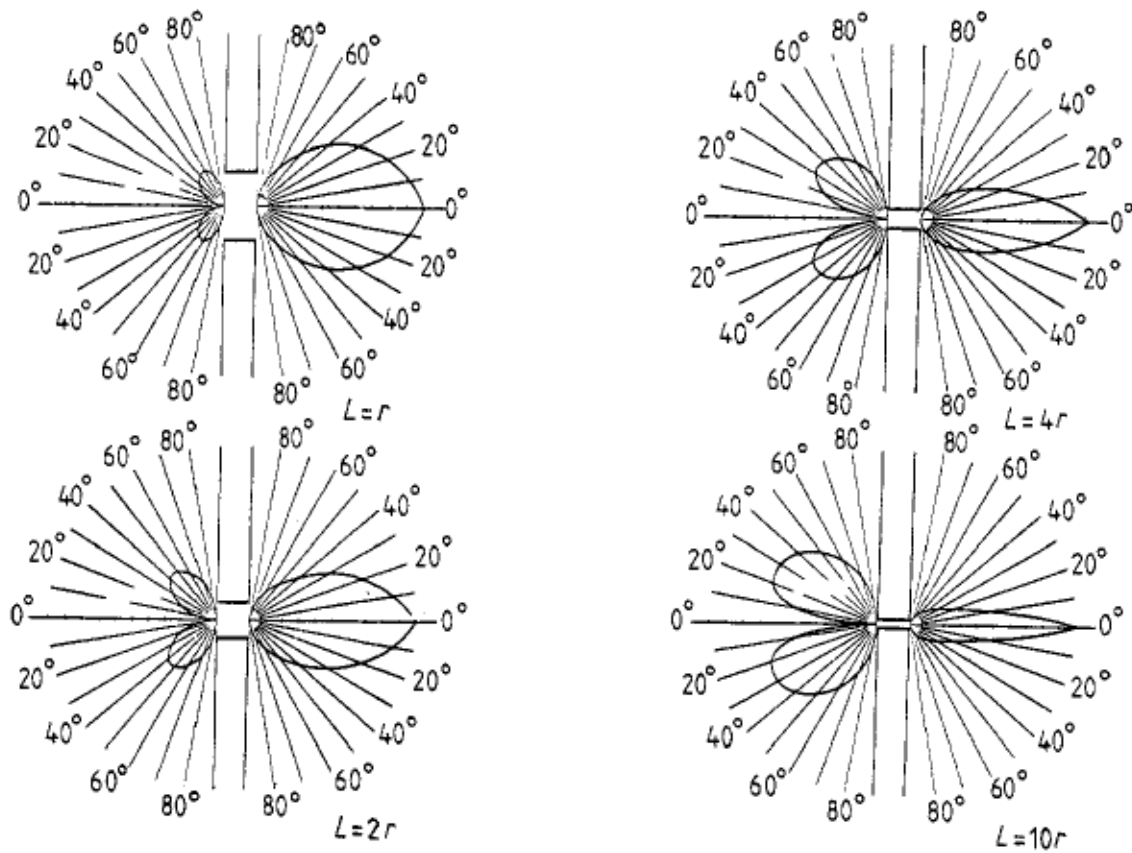

Fig. 3: Beaming effect for circular tubes of different length-to-radius ratios [4,6]

As soon as computers became available for this kind of calculation, they were used to calculate the transmission probability of simple and complex geometries, referring to real vacuum components, such as tubes, elbows, baffles, pumps [7,8]. All that needs to be done is to simulate the microscopic behaviour of the molecules under UHV conditions, with the assumption that their direction of emission follows the cosine law, frequently referred to as Lambert's law, i.e., that a molecule resting on a surface, has a probability dn/N of being desorbed within the solid angle $d\omega = \sin\theta \cdot d\theta \cdot d\phi$ as shown in Fig. (4), and given by

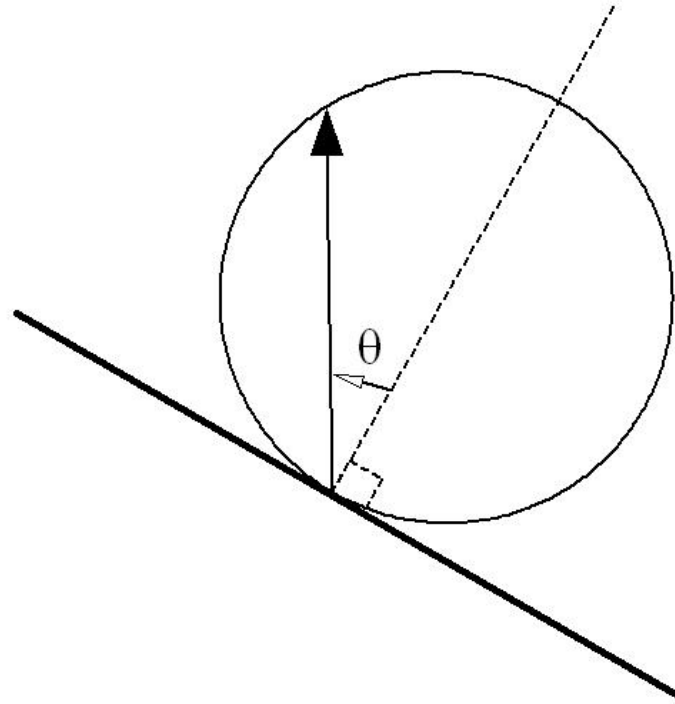$$\frac{1}{N}\frac{dn}{d\omega} = \frac{\cos\theta}{\pi} \quad .$$
(7)

Fig. 4: Definition of the zenith angle of emission θ following Lambert's law. The azimuthal angle φ is a rotation about the axis perpendicular to the plane.

2.2   The Monte Carlo method

The Monte Carlo (MC) method has been used extensively for this purpose, as shown in Ref. [9] and Ref. [10] and references therein. The MC algorithm under UHV conditions, frequently called the Direct Simulation Monte Carlo method (DSMC) generates molecules one by one and tracks them from 'source' to 'sink' [11].

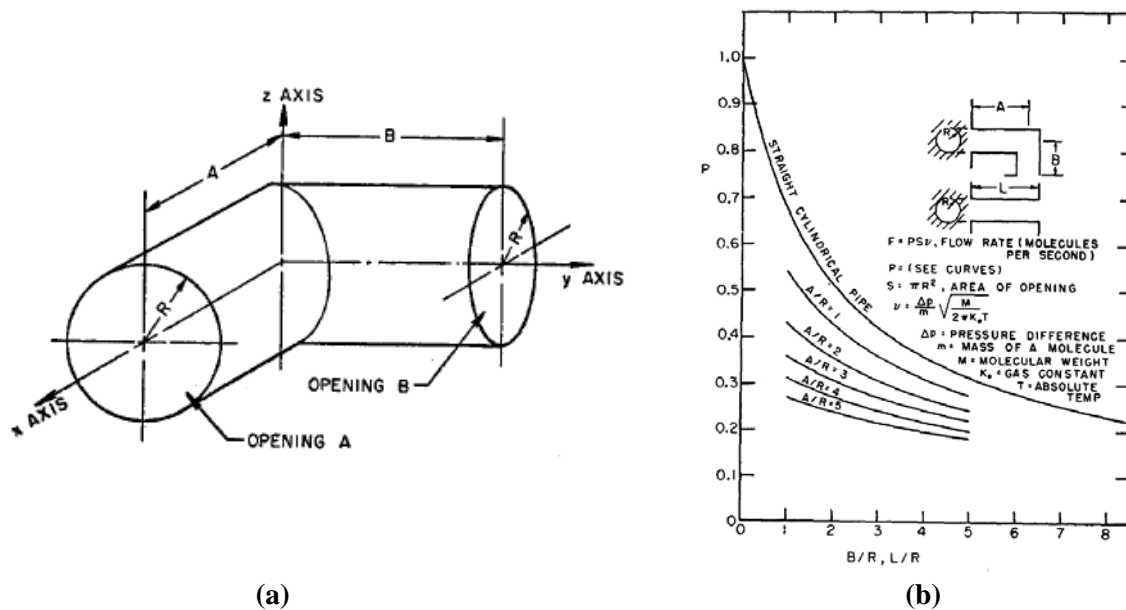Figures 5 and 6 show examples of such calculations.

(a)

(b)

Fig. 5: (a) Geometry for the MC simulation of an elbow; (b) its transmission probability [7]
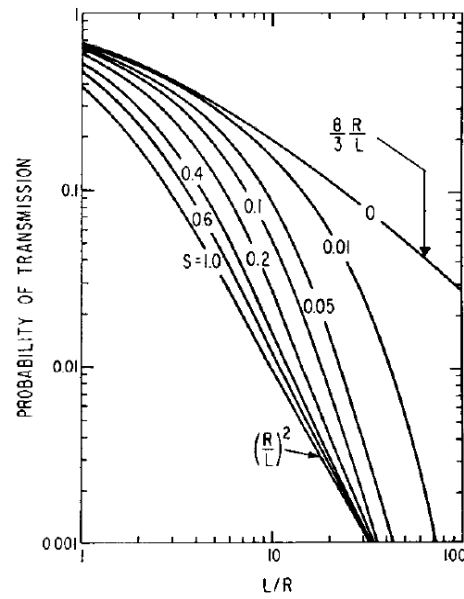
Fig. 6: Transmission probability for circular tubes of length *L* and radius *R* for different values of the sticking coefficient [8]

This can be generalized to any cross-section, such as the one for LEP, as shown in Fig. 7 [12] and modelled in Fig. 8 [10].
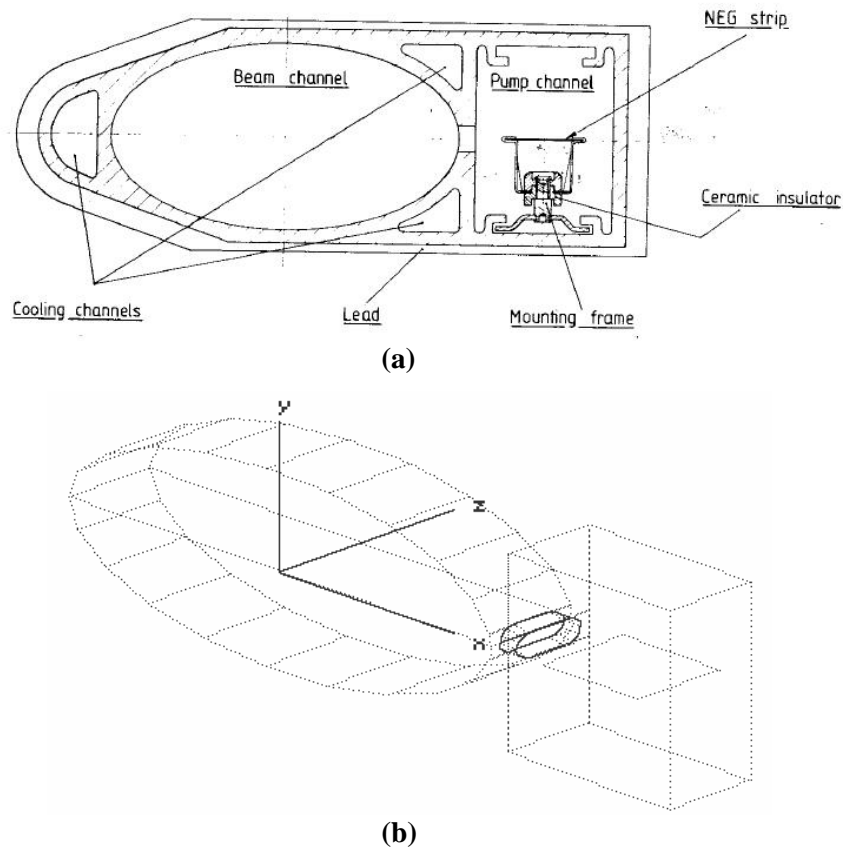

(a)

(b)

Fig. 7: (a) Cross-section of the dipole LEP chamber with NEG strip [12]; (b) Twenty-five mm long slice of the LEP chamber, with 20×9 mm^2 racetrack-shaped slot between chamber and antechamber [10,12].
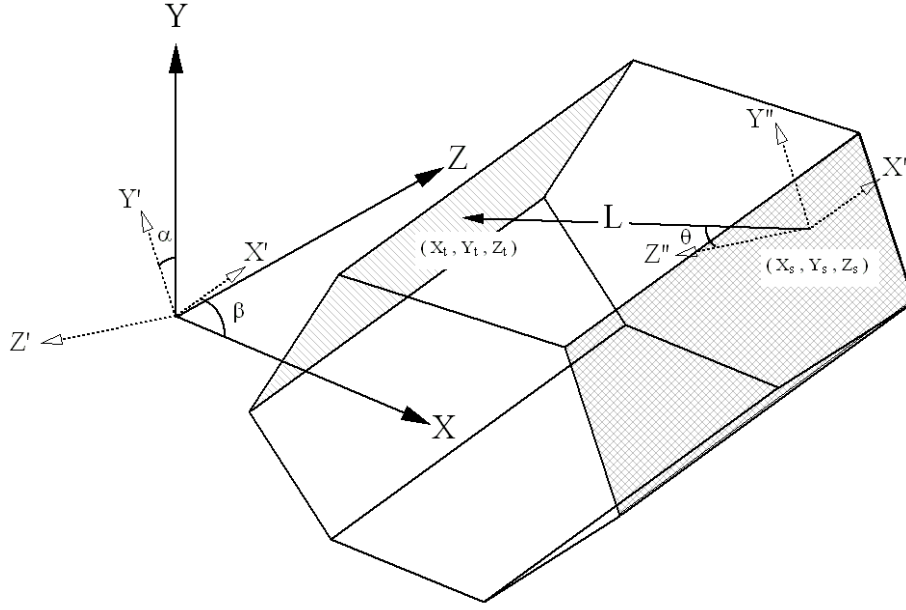
Fig. 8: Definition of some geometrical variables used for making a 3D MC simulation [10]

A three-dimensional (3D) description of the vacuum component is done. The easiest way is to make it up by using planar facets (polygons) as done in Refs. [10,11].

In this case, the ray-tracing calculation goes as follows, see Fig. 8:

- let XYZ be an arbitrary frame of reference;

- let $X''Y''Z''$ be the frame of reference whose origin corresponds to the the position of the molecules on a facet, with Z'' perpendicular to the facet (normal vector);

- let $X'Y'Z'$ be a frame of reference parallel to $X''Y''Z''$, with the same origin as XYZ;

- let β be the rotation angle about the Y axis which takes the X axis onto X', and α the one about X' which takes Z onto Z'.

The following transformation equations can be written

$$\begin{pmatrix} X'' \\ Y'' \\ Z'' \end{pmatrix} = \begin{pmatrix} 1 & 0 & 0 \\ 0 & \cos\alpha & \sin\alpha \\ 0 & -\sin\alpha & \cos\alpha \end{pmatrix} \cdot \begin{pmatrix} X' \\ Y' \\ Z' \end{pmatrix} , \tag{7a}$$

$$\begin{pmatrix} X \\ Y \\ Z \end{pmatrix} = \begin{pmatrix} \cos\beta & 0 & \sin\beta \\ 0 & 1 & 0 \\ -\sin\beta & 0 & \cos\beta \end{pmatrix} \cdot \begin{pmatrix} X'' \\ Y'' \\ Z'' \end{pmatrix} . \tag{7b}$$

A molecule at position (X_s, Y_s, Z_s) ('source') is generated with a desorption (zenith) angle θ following a cosine distribution with respect to Z'' (φ is the azimuthal angle of rotation about Z'', not shown on Fig. 8) according to the equations

$$\begin{cases} X'' = L\sin\theta\cos\varphi \\ Y'' = L\sin\theta\sin\varphi \\ Z'' = L\cos\theta \end{cases} . \tag{8}$$

291

The angle θ is obtained by generating a random number r with uniform distribution in the interval $[0,1]$, and then using the relation [13]

$$\theta = \sin^{-1}(\sqrt{r}) \quad .$$ (9)

The molecule will hit another facet at point (X_t, Y_t, Z_t) ('target')

$$\begin{cases} X_t = X_s + L_t(\sin\theta\cos\varphi\cos\beta_s - \sin\theta\sin\varphi\sin\alpha_s\sin\beta_s - \cos\theta\cos\alpha_s\sin\beta_s) \\ Y_t = Y_s + L_t(\sin\theta\sin\varphi\cos\alpha_s - \cos\theta\sin\alpha_s) \\ Z_t = Z_s + L_t(\sin\theta\cos\varphi\sin\beta_s + \sin\theta\sin\varphi\sin\alpha_s\cos\beta_s + \cos\theta\cos\alpha_s\cos\beta_s) \end{cases}$$ (10)

with L_t given by

$$\begin{cases} L_t = -(A_t X_s + B_t Y_s + C_t Z_s + D_t)/U \\ U = A_t(\sin\theta\cos\varphi\cos\beta_s - \sin\theta\sin\varphi\sin\alpha_s\sin\beta_s - \cos\theta\cos\alpha_s\sin\beta_s) + \\ \quad + B_t(\sin\theta\sin\varphi\cos\alpha_s - \cos\theta\sin\alpha_s) + \\ \quad + C_t(\sin\theta\cos\varphi\sin\beta_s + \sin\theta\sin\varphi\sin\alpha_s\cos\beta_s + \cos\theta\cos\alpha_s\cos\beta_s) \end{cases} \quad .$$ (11)

With A_t, B_t, C_t and D_t the coefficients defining the plane $A_tX + B_tY + C_tZ + D_t = 0$ which contains the polygon defining facet t. The MC code is such that it calculates L_t for each facet defining the model of the vacuum system except the source one, and then takes as the good L_t the one corresponding to the shortest positive L_t. It then repeats the procedure until a molecule is adsorbed by a surface: this is accomplished by assigning to each facet a sticking coefficient corresponding to the pumping speed of that facet. The sticking coefficient is the probability that a molecule hitting a facet will be permanently pumped. The relationship between sticking coefficient s and pumping speed S (l/s) of a facet is given by Eq. (12)

$$S = s \cdot A \cdot \frac{\bar{v}}{4}$$ (12)

which has the same form as Eq. (5), with the sticking coefficient s taking the place of the transmission probability $P_{i \to j}$ and the pumping speed S the place of the conductance C. A 1 cm^2 surface with $s = 1$, i.e., a perfect pump, has a pumping speed S of 11.77 l/s/cm^2 for N_2 (or CO) at a temperature of 20°C.

The transmission probability w follows a binomial distribution with a standard deviation (N = number of generated molecules) [10, 14,15]

$$\sigma = \sqrt{\frac{w \cdot (1-w)}{N}} \quad .$$ (13)

The conductance C of a tube of any cross-section is obtained by calculating w using the DSMC method, and then inserting it in place of $P_{i \to j}$ into Eq. (5). The standard deviation of C follows immediately from that of w.

For a MC simulation to be effective, it is of paramount importance to use an appropriate random number generator (RNG). It must have a suitably large period, in order to avoid that the generated number be correlated, thus skewing the results. For some high-precision simulations, where billions of molecules need to be generated in order to reduce the statistical error, the RNGs can have periods as large as $2^{19937} \sim 10^{6000}$ [14,15].

2.3   Comparisons

References [4,5,9] can be used in order to check the relative accuracy of the different methods discussed so far. In general, for tubes of constant circular cross-section, most methods agree to a few per cent, with notable deviations when the length-to-radius ratio becomes small. For chambers with complicated cross-sections (chamber–antechamber, coaxial tubes, triangular or rectangular profiles) the deviations become more and more pronounced. See Section 3.9 for further comments on this.

3   Pressure profile calculations

After having reviewed the concept of conductance and some of the methods which can be used to calculate it for a system of given geometry, we can now move on to look at the different ways of calculating pressure profiles.

Since most accelerators or accelerator components (e.g., beamlines) have one dimension which is much bigger than the two others (circumference or beamline length vs cross-section of the chamber), a good starting point is to consider a uni-dimensional mass-balance equation of the type

$$V \frac{dP(x,t)}{dt} = Q(x,t) - S(x,t) \cdot P(x,t) + c(x,t) \cdot \frac{d^2 P(x,t)}{dx^2} \tag{14}$$

where V is the volume, P the pressure, Q the outgassing yield, S the pumping speed, and c the specific conductance in litres·m/s.

Most particle accelerators run under conditions which can be thought of as a steady state: a given beam is injected into the machine, and then circulates in it for times that are normally much longer than the time taken by the molecules to move along the chamber and be pumped. As we have seen in Eq. (6), these average speeds are of the order of several hundred metres per second, and therefore any changes in the conditions of the machine (beam current and energy, beam position) which happen on a time scale longer than, say, a few seconds, can be considered as stationary from the point of view of pressure. The time evolution of the pressure can therefore be neglected, thus simplifying the analysis. Equation (14) then becomes

$$c(x) \cdot \frac{d^2 P(x)}{dx^2} - S(x) \cdot P(x) = -Q(x) \ . \tag{15}$$

In the literature, it is solutions to this equation that are found most often. Some of them are obtained analytically, others numerically.

Looking at Eq. (15) it becomes clear now why we have discussed the conductance before coming to this point. Together with the pumping speed, it is the conductance which determines the shape of $P(x)$. We will see that S could in principle be made very large (at least locally), while c has an upper bound due to the physical dimension of the accelerator, mainly the physical aperture of the magnets. This fact is often referred to by saying that accelerators are conductance-limited systems.

3.1   Analytic solutions

When c and S are constants, a solution can easily be obtained by integrating the second-order differential equation (15).

The simplest model to start with is the one represented by a vacuum chamber of constant cross section, with a uniform outgassing yield q (in mbar · l/s/cm^2), a number of lumped pumps equally spaced L metres apart, and no distributed pumping. It can be thought of as a periodic system, with

period equal to the spacing of the pumps. Let A be the specific surface of the vacuum chamber A, in cm^2/m, as indicated by the example shown in Fig. 9.

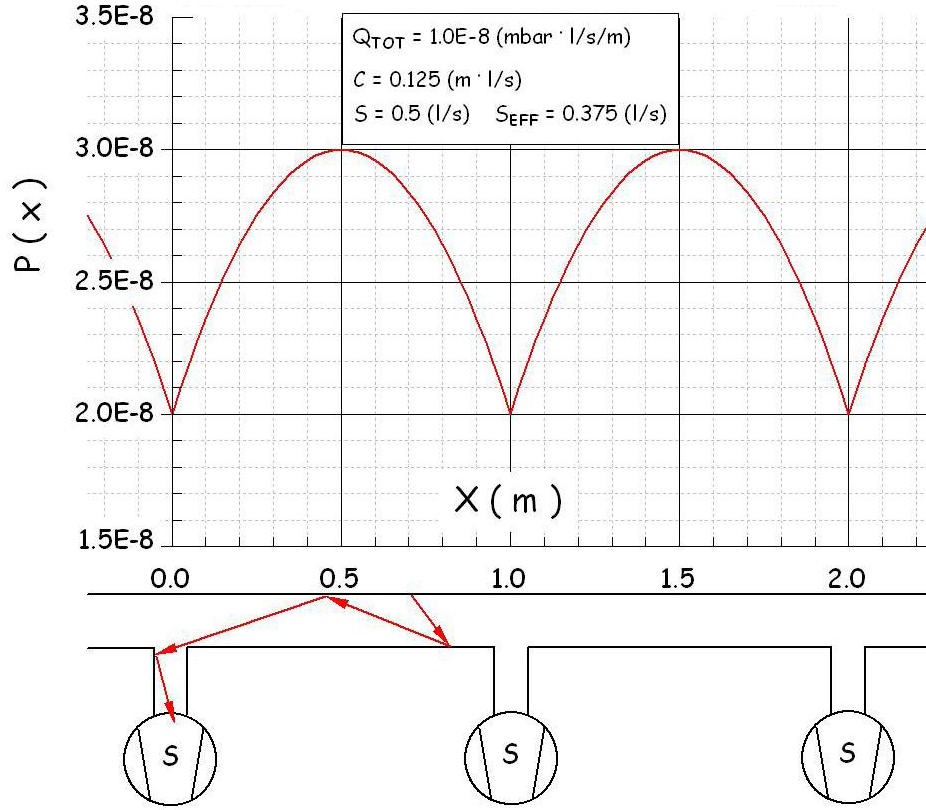$$c\frac{d^2 P(x)}{dx^2} = -Aq \quad . \tag{16}$$

Fig. 9: Pressure profile for a periodic system

By symmetry, the boundary conditions are

$$\begin{cases} \dfrac{dP}{dx}(x = L/2) = 0 \\ P(x = 0) = AqL/S \end{cases} \quad . \tag{17}$$

The solution is

$$P(x) = \frac{Aq}{2c}(Lx - x^2) + \frac{AqL}{S} \quad . \tag{18}$$

The average and the maximum pressures, which can be relevant for the operation of the accelerator, are given by

$$\begin{cases} P_{avg} = \dfrac{1}{L}\displaystyle\int_0^L P(x)dx = AqL(\dfrac{L}{12c} + \dfrac{1}{S}) = AqL(\dfrac{1}{S_{eff}}) \\ P_{max} = AqL(\dfrac{L}{8c} + \dfrac{1}{S}) \end{cases} \quad , \tag{19}$$

with S_{eff}, the effective pumping speed, given by

$$S_{\text{eff}} = (\frac{L}{12c} + \frac{1}{S})^{-1} \quad . \tag{20}$$

It now becomes evident why accelerators are said to be conductance-limited systems. There is no point in increasing the pumping speed S beyond few times c/L, since even for a very large S the effective pumping speed would be limited to $12 \cdot c/L$, as indicated in Fig. 10.
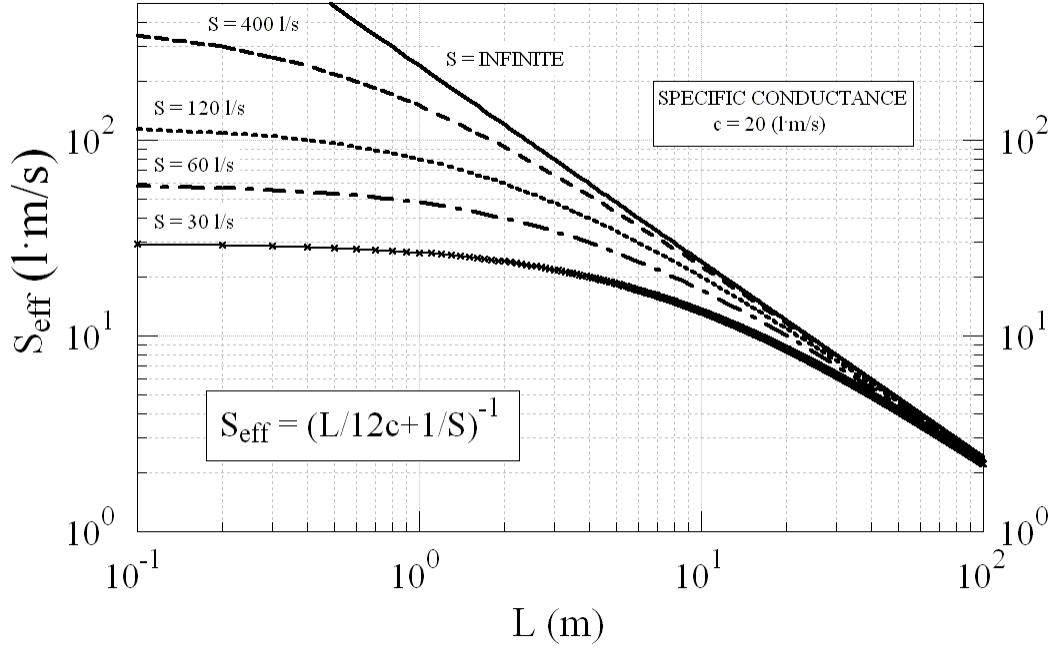

Fig. 10: Effective pumping speed vs pump spacing, for selected values of the specific conductance

As an example, let us consider the case of the ESRF: at a nominal beam current $I = 200$ mA, and energy $E = 6$ GeV, the total photon flux F is

$$F = 8.08 \cdot 10^{17} \cdot E \cdot I \qquad \text{(ph/s)} \quad . \tag{21}$$

For a well-conditioned system, a value of the photodesorption yield η of 10^{-6} mol/photon can be reasonably assumed [16], which gives a total outgassing rate of $Q = F \cdot \eta \cdot k$, where $k = 4.047 \times 10^{-20}$ mbar $\cdot$ l/molecule, or $Q = 3.53 \cdot 10^{-5}$ mbar $\cdot$ l/s. Using Eq. (1), we obtain S as a function of Q and P, the measured average pressure. For the ESRF, a typical average pressure during operation is $1.5 \cdot 10^{-9}$ mbar, which yields $S = 3.53 \cdot 10^{-5}/1.5 \cdot 10^{-9} \approx 23\,500$ l/s. This would be the total pumping speed to install along the storage ring were not the system conductance limited. The real installed pumping speed, on the other hand, is ~ 4700 l/s per standard cell. Since there are 32 cells in the ESRF, the total goes to $\sim 150\,000$ l/s, or ~ 6.5 times the value calculated by using Eq. (1).

If either c, Q, S, or L are not constant, then 'piece-wise' solutions can be found [16]. In this case the pressure profile looks like a series of parabolae. It should be kept in mind that this solution is only approximate, since it does not take into account the effect of the changes of the cross sections.

If the distributed pumping speed is not zero throughout the system, then Eq. (15) becomes ($Aq = Q$, specific gas load in mbar $\cdot$ l/s/m)

$$c\frac{\mathrm{d}^2 P(x)}{\mathrm{d}x^2} + Q - SP = 0 \quad . \tag{22}$$

Its solution is given by

$$P(x) = \frac{Q}{S} + Ae^{\sqrt{\alpha}} + Be^{-\sqrt{\alpha}} \tag{23}$$

where $\alpha = S/c$. The solution is of an hyperbolic sine/cosine type. The boundary conditions between areas with distributed pumping and areas with lumped pumping, or no pumping at all, are given by the continuity of $P(x)$ and its first derivative $\mathrm{d}P/\mathrm{d}x$ at the boundaries. If the vacuum chamber is 'sliced' into N sections, and each section has its own c_i, Q_i, S_i and P_i, then the boundary conditions give $2N$ equations with $2N$ unknowns, which can be solved.

As an example, taken from Ref. [16], the pressure profile along one cell of a particle accelerator, calculated using this method, is shown in Fig. 11.
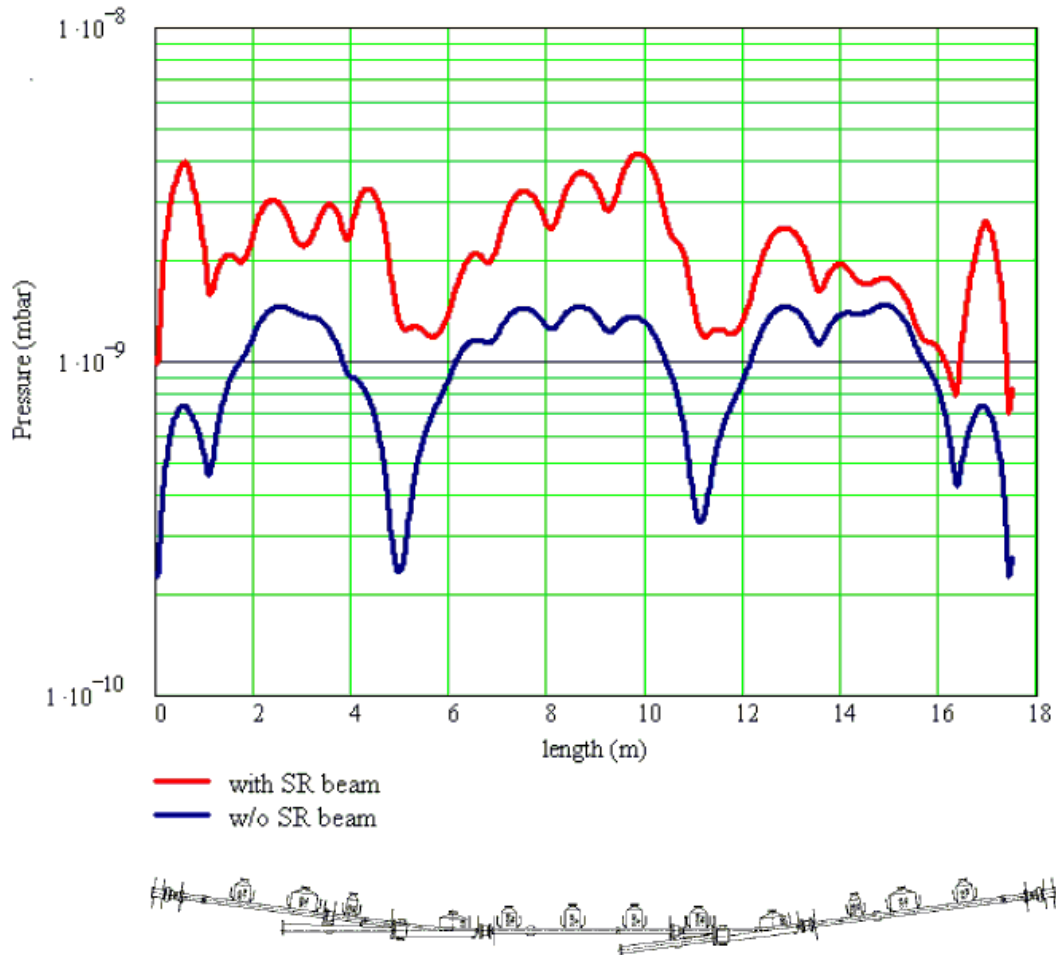

Fig. 11: Pressure profile along one cell of Diamond [16]

3.2   Transfer-matrix method

Under the assumption that c, S and Q are piece-wise constants, Eq. (22) and its solution Eq. (23) can be solved by using algorithms which are implemented in machine lattice codes such as

TRANSPORT [17], where the particle beam is tracked through the magnetic lattice. In this case, a corresponding 'vacuum lattice' is thought of [18,19], which obeys equations of the type

$$
\begin{pmatrix} P(L) \\ dP(L)/dz \\ 1 \end{pmatrix} = \begin{pmatrix} \cosh(\alpha L) & \dfrac{\sinh(\alpha L)}{\alpha} & -\dfrac{q}{c}\dfrac{\cosh(\alpha L)-1}{\alpha^2} \\ \alpha\sinh(\alpha L) & \cosh(\alpha L) & -\dfrac{q}{c}\dfrac{\sinh(\alpha L)}{\alpha} \\ 0 & 0 & 1 \end{pmatrix} \cdot \begin{pmatrix} P_0 \\ dP_0/dz \\ 1 \end{pmatrix}
\tag{24}
$$

with c, s and α as defined above. This equation maps the initial pressure and gradient, P_0 and dP_0/dx, to their values after a length $z = L$.

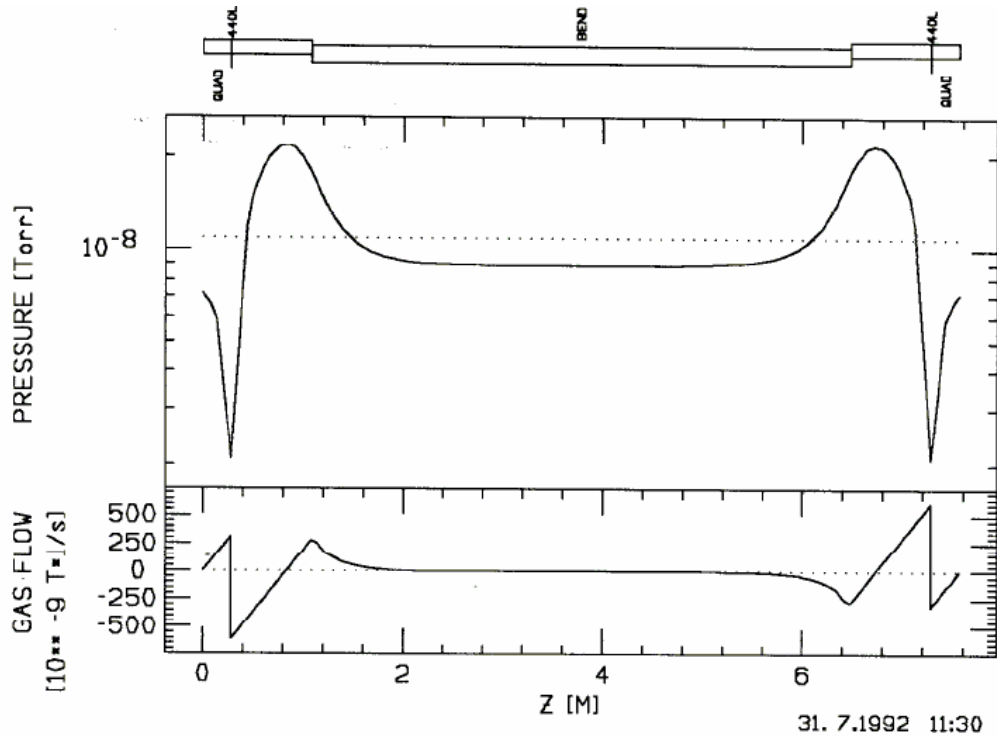An example is shown in Fig. 12, taken from Ref. [18].

Fig. 12: Pressure profile and its gradient calculated with VAKTRAK [18]

A similar approach has been used in Ref. [20], where Eq. (22) is re-written as

$$
\frac{d}{dx}\left(c\frac{dP}{dx}\right) - SP + Q = 0 \; .
\tag{25}
$$

In this case c, S and Q can vary. A solving technique based on the finite-difference method is used, after discretization of the system (slicing) into N parts

$$
\frac{d}{dx}\left(c_i\frac{dP}{dx}\right) = \frac{(c_{i+1}-c_{i-1})P_{i+1} + (c_i - c_{i-1})P_{i-1}}{2\Delta x^2} - \frac{(c_{i+1}-c_{i-1}+2c_i)P_i}{2\Delta x^2} \; .
\tag{26}
$$

This, together with the boundary conditions

$$Q_i = -c_i \frac{P_{i+1} - P_{i-1}}{2\Delta x^2} \tag{27}$$

becomes a tri-diagonal matrix which is multiplied by the pressure vector Pi. A solution can be found by employing, for instance, a Gaussian elimination and back-substitution technique, an example of which is shown in Fig. 13.
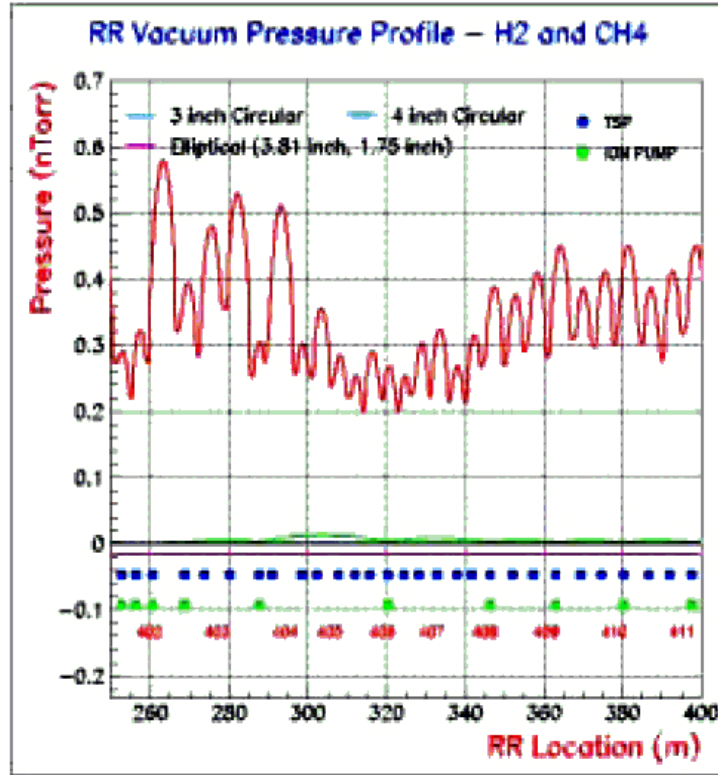

Fig. 13: Pressure profile along FNAL's Recycler Ring [21]

3.3 The continuity principle of gas flow

Another way of solving the mass-flow balance equation is the so-called Continuity Principle of Gas Flow (CpoGF), which can be stated after discretization of the vacuum system as per Fig. 14.
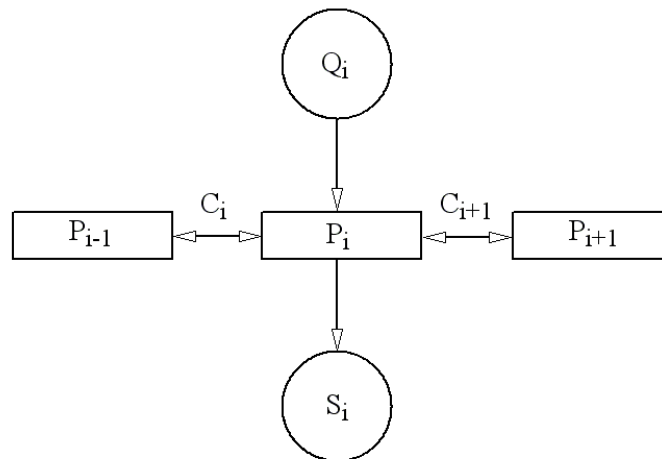

Fig. 14: The continuity principle of gas flow [22]

Each segment of the vacuum system is assigned its S_i, Q_i and C_i, and then its pressure P_i is obtained by solving the set of equations

$$c_i(P_{i-1} - P_i) + c_{i+1}(P_{i+1} - P_i) + Q_i = S_i P_i \quad . \tag{28}$$

Several types of boundary conditions (BC) can be thought of [22]:

– Periodic BC:

$$\begin{cases} P_0 = P_n \\ P_{n+1} = P_0 \end{cases} \tag{29}$$

which introduced into Eq. (28) gives

$$\begin{cases} C_1(P_n - P_1) + C_2(P_2 - P_1) + Q_1 = S_1 P_1 \\ C_i(P_{i-1} - P_i) + C_{i+1}(P_{i+1} - P_i) + Q_i = S_i P_i \\ C_n(P_{n-1} - P_{n1}) + C_1(P_1 - P_n) + Q_n = S_n P_n \end{cases} \tag{30}$$

where $i = 2, 3, \ldots (n-1)$.

– Smooth BC:

$$\begin{cases} P_0 = P_1 \\ P_{n+1} = P_n \end{cases} \tag{31}$$

which introduced into Eq. (28) gives

$$\begin{cases} C_2(P_2 - P_1) + Q_1 = S_1 P_1 \\ C_i(P_{i-1} - P_i) + C_{i+1}(P_{i+1} - P_i) + Q_i = S_i P_i \\ C_n(P_{n-1} - P_{n1}) + Q_n = S_n P_n \end{cases} \tag{32}$$

where $i = 2, 3, \ldots (n-1)$.

– Fixed-pressure BC:

When P_0 and P_n are known (or set to a given value), Eq. (28) becomes

$$\begin{cases} -C_1 P_1 + C_2(P_2 - P_1) + (Q_1 + C_1 P_0) = S_1 P_1 \\ C_i(P_{i-1} - P_i) + C_{i+1}(P_{i+1} - P_i) + Q_i = S_i P_i \\ C_n(P_{n-1} - P_{n1}) - C_1 P_n + (C_{n+1} P_{n+1} + Q_n) = S_n P_n \end{cases} \tag{33}$$

where $i = 2, 3, \ldots (n-1)$.

The 3 BC cases can be solved by a forward substitution and chase-back technique [22], to obtain the pressure profile of Fig. 15.
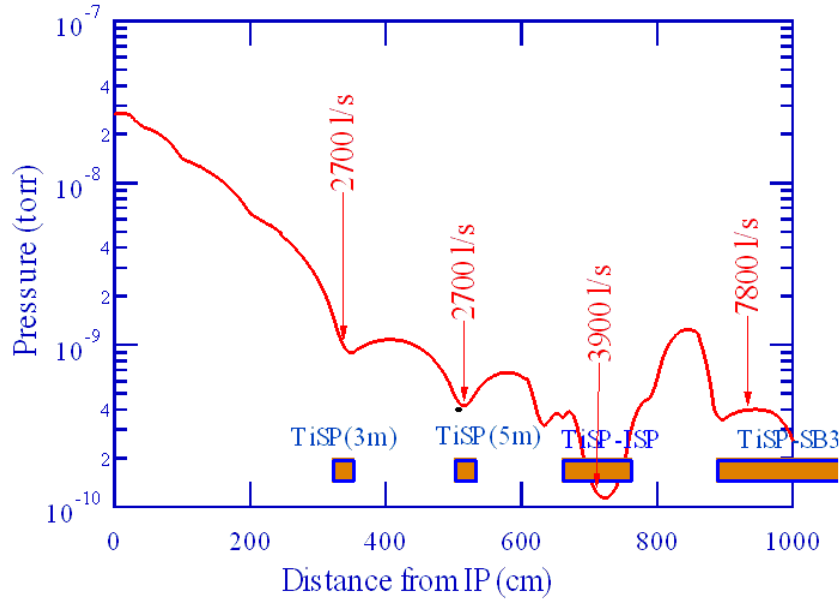
Fig. 15: The CPoGF algorithm applied to the interaction region of CESR-III – CLEO-III. IP = Interaction Point; TiSP = Titanium Sublimation Pump [22]

3.3.1 Commercial programs

Commercial programs have been used by some authors to calculate vacuum pressure distributions: examples are the use of MathCad, for analysing the pressure inside a RF waveguide [23–25].

3.4 Time-dependent analytic calculations

It may be interesting to calculate time-dependent pressure profiles, such as when the effect of gas leaks or a sudden air in-rush need to be calculated. One possible way of solving the problem is to start with the equation [26]

$$c\frac{\partial^2 P(x,t)}{\partial x^2} = -q(x,t) + v\frac{\partial P(x,t)}{\partial t} \tag{34}$$

where v is the specific volume (volume per unit length of the system), and q the specific outgassing yield.

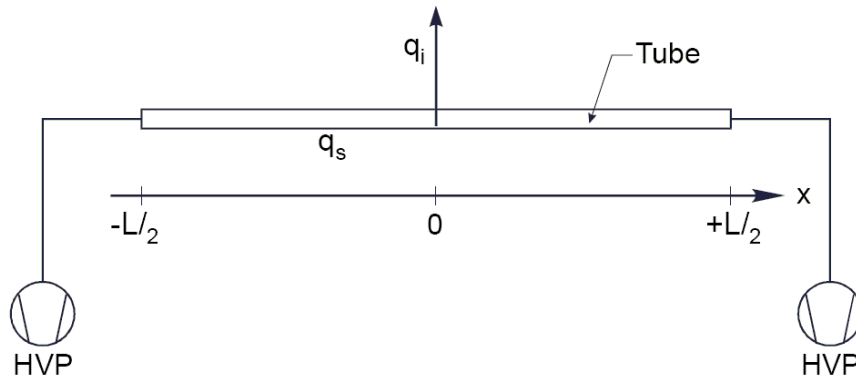As an example let us consider the case of Ref. [26], depicted in Fig. 16:

Fig. 16: Tube of length L pumped at the extremities, with a pulsed localized leak q_i in the middle of it, and one high-vacuum pump (HVP) at each end [26]

300

If the localized pulsed leak q_i is described by the equation $q_i(x,t) = q'\delta(x)\delta(t)$, then Eq. (34) can be solved analytically as

$$P(x,t) = -\frac{q}{2c}x^2 + \frac{Q_T}{2}\left(\frac{1}{S} + \frac{L}{4c}\right) + \frac{q'}{\sqrt{4\pi cvt}}\exp\left(-\frac{v}{4ct}x^2\right) \quad . \tag{35}$$

Where the first part of the equation is the parabolic pressure profile due to a spatially uniform outgassing yield q [similar to Eq. (18)], and the second part comes from the gas burst q'. With reference to the geometry of Fig. 16, the solution to this equation is shown in Fig. 17.
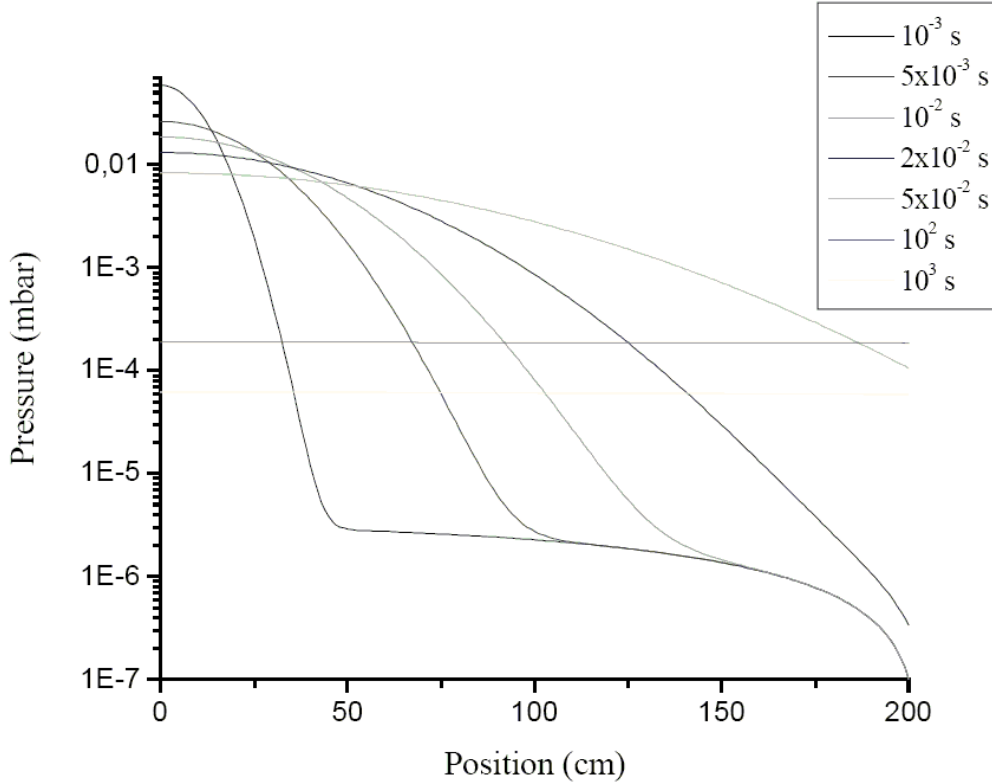

Fig. 17: Solution to Eq. (35) when $L = 400$ cm, $q' = 0.01$ mbar $\cdot$ l, $q = 4.7 \cdot 10^{-8}$ mbar $\cdot$ l/s/cm [26]

3.5   The Monte Carlo method

We have already introduced in Section 2 the main features of the MC method, for the calculation of transmission probabilities. There is not much else that needs to be done to use this method for calculating pressure profiles. A geometrical description (model) of the system is made, and then the MC simulation program is started. We have seen that for the calculation of transmission probabilities the molecules are made to desorb from one end of the system, usually a tubular geometry, and the program tracks all molecular trajectories and computes the fraction of the molecules which reach the other end. For the pressure profile calculation, for an accelerator the source of gas is, more often than not, distributed along the chamber in ways that depend on many factors, such as the type of accelerator (synchrotron radiation (SR) light source, high-energy hadron machine, linac, etc.), and the particular situation or mode of operation (fixed energy vs ramped, pulsed machine, gas leak, etc.).

Therefore, it is a pre-requisite to the MC calculation to calculate the desorption profile along the chambers. It should be clear that the accuracy of the result will then depend not only on the statistical accuracy of the MC algorithm, but also on the accuracy of the estimation of the desorption profile. As

an example, for a SR light source one could be tempted, as a first approximation, to set the desorption profile proportional to the photon flux of Eq. (21). This would not take into account the fact that it is not only the instantaneous photon flux which matters, but the integrated photon flux D_γ as well, i.e., how many photons have hit a particular region of the chamber in the past. The instantaneous photon flux F at each point of the vacuum chamber needs to be multiplied by the correct photodesorption yield η, which is a function of D_γ [16]. The calculation of F can be accomplished by performing a ray-tracing analysis, or by using some analytic formulae [27]. Clearly, this needs to be done in close relationship with machine-physics experts, who can advise on the orbit trajectories and properties (emittances, beta functions, dispersion, etc.) [28]. The coefficient η can be obtained by measurement, or extrapolated from data in the literature [16].

Let us now go back to the MC calculation of pressure profiles. All programs which have been written so far [7–12] work on the common principle of tracking a large number of molecules and keeping a record of all molecular hits on the surfaces making up the model of the vacuum system under study. The advantage of this method as compared to those discussed previously, is that it does not need the prior computation of the conductances or effective pumping speeds. In fact, it will calculate these quantities as a by-product of the calculation of the pressure profiles.

One example will clarify this point. Figure 18 (a) shows the 3D model made with Molflow of a side pumping-port which is located on the dipole chambers of the ESRF. Each chamber has two such pumping ports which stick out of the magnet yoke, between the magnet coils. There is first a narrow rectangular box which is welded on one side to a conical taper that goes into a CF63 flange, where one pump is connected. Both the rectangular box and the conical taper have some internal reinforcing ribs in order to prevent collapse due to external pressure. On the opposite side, near the dipole chamber, there are five rectangular slots machined onto a thick stainless steel bar which constitutes the backbone of the dipole chamber. One pumping port has a 60 l/s ion-pump installed on it, the other one a 200 l/s NEG pump. The MC calculation is done in order to find the conductance of each pumping port, which then yields the effective pumping speeds at the beam chamber. It also gives the pressure drop between the beam chamber and the pumps' inlets. Figure 18 (b) shows this pressure profile (solid line). The circular facet in A, the pump inlet, has a sticking coefficient of 1 (ideal pump), which corresponds to an installed pumping speed of 914 l/s [Eq. (12) for 20ºC CO gas]. The pressure profile is calculated for a unitary outgassing yield: the reciprocal of the vertical scale is therefore the effective pumping speed at the corresponding point on the horizontal axis, via the relation $S = Q/P$ derived from Eq. (1). This means that the effective pumping speed at point B is $1/0.0053 = 188.7$ l/s. The pressure at the pump inlet A derived from the graph is $1/0.0004 = 2500$ l/s, while it should be $1/914 = 0.00109$: the discrepancy is due to the fact that the pressure under molecular flow conditions is not isotropic [9], it depends on the direction of measurement. Figure 19 shows the angular distribution of incident angles at the circular section between the taper and the pump inlet, 53 mm in front of the pump inlet circle. The large departure from the cosine-like distribution is evident. The transparent facet A–B is perpendicular to the average flow of molecules from C–D. The circular facet in A, the one that simulates the 914 l/s pump inlet, gives the correct value for the pumping speed, since it has a pressure of 0.001094 after 1 990 000 molecules have been generated.

One advantage of the MC method is the possibility of changing the microscopic properties of, for instance, the vacuum surfaces [29], and seeing what impact this has on the pressure profile or transmission probability of the system. It allows the exploration of 'what if' scenarios, such as finding out what changes would take place if the theoretical cosine-like desorption from vacuum surfaces were replaced by another angular distribution. Or, it can be used to simulate the desorption from a facet which takes the place of the exit of a tubular structure (like a gas injection manifold, for instance): in this case, the desorption from the facet takes a $\cos^n \theta$ power law, in order to simulate the beaming profile, with the power exponent n extrapolated from data such as those in Fig. 3 or Fig. 19.
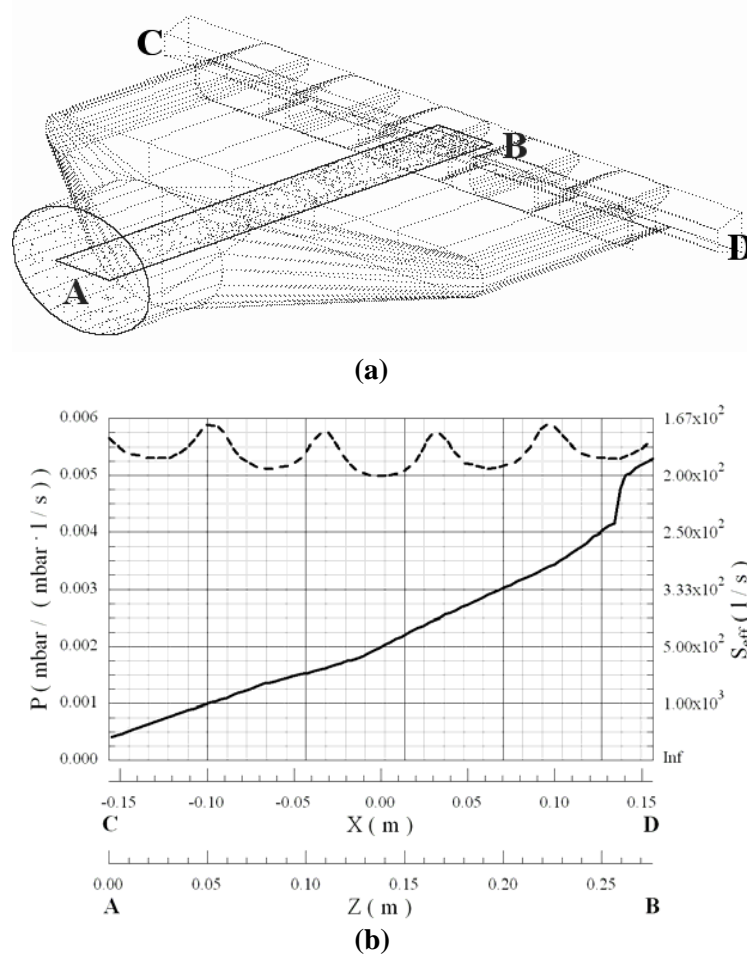
(a)

(b)

Fig. 18: (a) Molflow model of one ESRF dipole pumping port; Point A = pump's inlet; B = beam chamber. Molecules are generated along the beam chamber C–D. The rectangular facet A–B is a transparent facet used to keep track of the molecular hits (small dots). (b) Solid line: pressure profile along the pumping port, from A to B, Z scale; Dashed line: pressure profile along the beam chamber, from C to D, X scale.
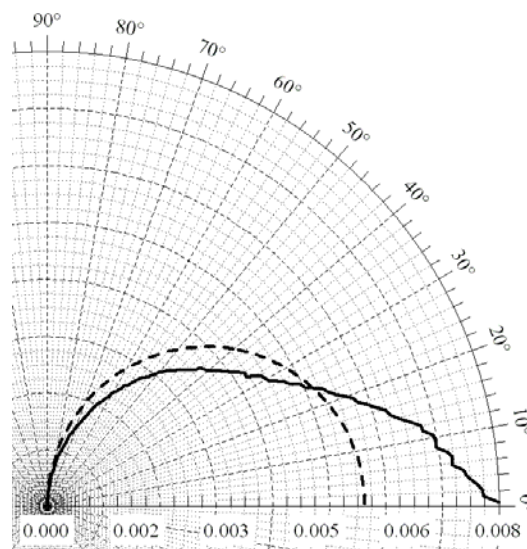

Fig. 19: Angle of incidence profile (solid line) compared to a cosine-like (dashed line). The 0° line is the normal vector to the pump inlet. The beaming effect is evident.

3.5.1   Time-dependent DSMC

There may be interest in simulating the time-dependent behaviour of gas species under UHV conditions. One way to do this is to follow the example set in Ref. [30]. The lengths of the molecular trajectories are translated into time intervals by means of the average molecular velocity given in Eq. (6). A suitable trajectory length step L_0 is chosen, corresponding to a time-step of $\tau_0 = L_0 / \bar{v}$. A large number of molecules are generated, to get statistical accuracy, and the position of the molecules at each time-step interval is recorded. Figures 20 (a) and 20 (b) exemplify this with clarity.
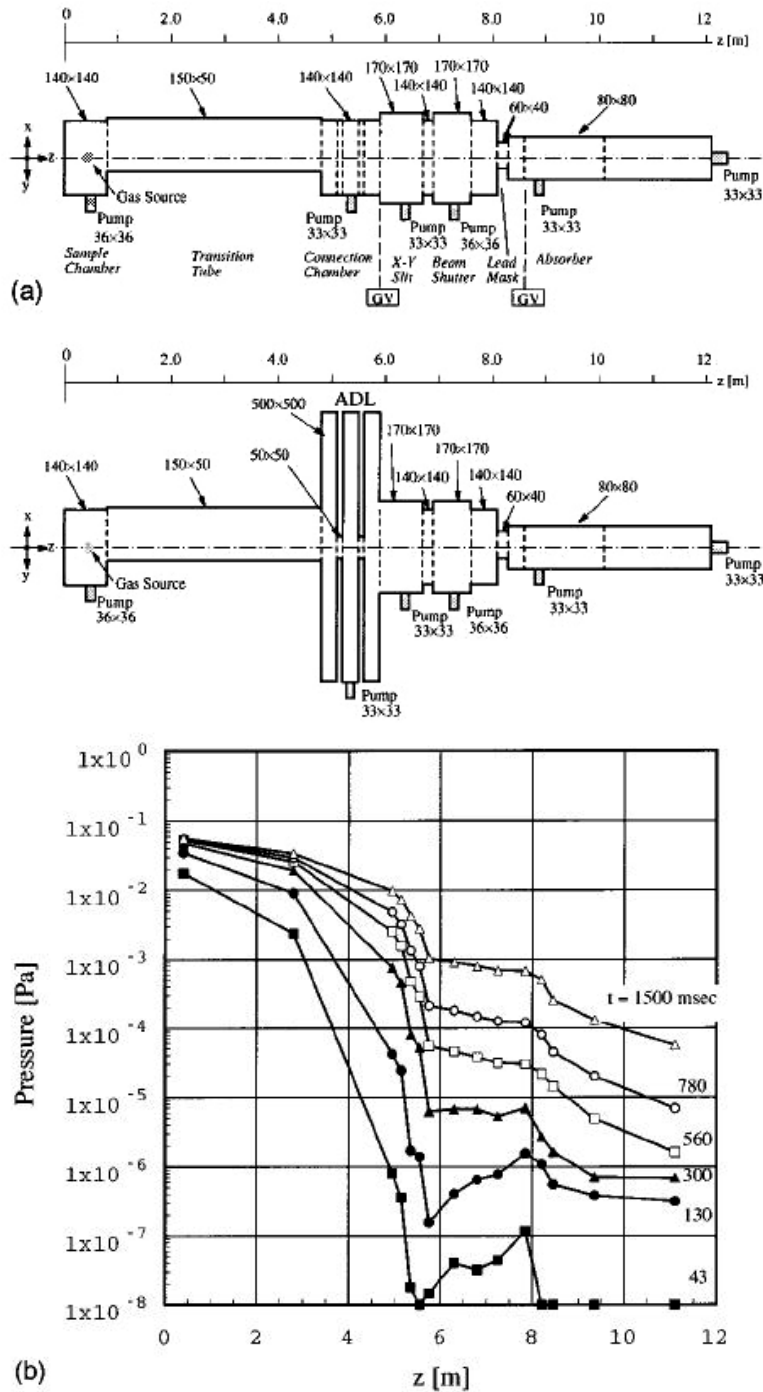

Fig. 20: Time-dependent MC simulation of an acoustic delay line (ADL) [30]; (a): geometry and dimensions of the ADL; (b): time-dependent pressure profiles

3.5.2   *Commercial products*

Instead of coding the MC ray-tracing algorithm using some high-level languages (Fortran, C, Pascal) [10–12], some authors have left the burden of making the 3D model and the ray-tracing calculations to some commercial programs [25]. In this case, one or more script files have to be created, and then the symbolic processor computational engine takes charge of tracking the molecular trajectories, storing the data, and post-processing them in order to visualize the results. The obvious advantage is that the user does not need to write hundreds of lines of code, the disadvantage is that the software licence can be expensive and the training time to become proficient in using the software can be long.

3.6   Diffusion equation

Several authors [31–33] have used the diffusion equation method in order to calculate both steady-state and time-dependent pressure profiles. The uni-dimensional diffusion equation is of the type [5,9]

$$\frac{\mathrm{d}n}{\mathrm{d}t} = D\frac{\partial^2 n}{\partial x^2} \tag{36}$$

where D is the diffusion coefficient of the gas specie under study, where n, the molecular density has been used instead of the pressure P. The equation $P = nkT$ gives the relationship between these two quantities. The diffusion coefficient D is related to the average molecular velocity and to the mean free path λ through the relationship $D = 1/3 \cdot \bar{v} \cdot \lambda$. Some interesting papers and analyses of vacuum systems of particle accelerators have been made using this method [31–33]. It is useful when the system under study can be thought of as being uni-dimensional. This means that the details of the pressure or density distributions at points where the local geometry of the system is important, cannot be obtained by this method. An example of this could be the geometry of a pumping port, or the side connection of a vacuum gauge to a vacuum chamber. Once solved, Eq. (36) could give the value of P or n at any given point in space and time (x,t), but the relationship between this and the pressure value read on a gauge attached to the chamber via a 'tee' or an elbow would need to be calculated separately, for instance using a MC algorithm.

3.7   Gas dynamics models

It is beyond the scope of this paper, which deals mainly with the case of molecular flows, to discuss the application of gas dynamics methods, which are more suited to describing the flow of gases at small Knudsen numbers. Since a dedicated lecture at this school has covered the subject (see F. Sharipov's lecture), it is just worth while to say that the integro-differential kinetic equation method (Ref. [34] and references therein) could certainly model a vacuum system under UHV conditions.

3.8   The view-factor (VF) or angular coefficients method

It has been realized that there is a mathematical analogy between the laws of molecular flow in systems with surfaces which desorb diffusively (cosine-like) and the radiative exchange of heat between walls at given temperatures [9,16].

For two sufficiently small surfaces, as depicted in Fig. 21 the following relation can be written for the molecular flux incident on any surface i

$$v_{\mathrm{inc}} = \sum_{j=1}^{n}(\varphi_{i\to j}\cdot v_j) \tag{37}$$

which leads to the system of algebraic equations

$$v_i = v_{0i} + (1 - \varepsilon_i) \cdot \sum_{j=1}^{n} (\varphi_{i \to j} \cdot v_j) = v_{0i} + (1 - \varepsilon_i) \cdot v_{inc} \quad . \tag{38}$$

The coefficients ε_i are taken as sticking probabilities. The $\varphi_{i \to j}$ are the angular coefficients and

$$v_{ads} = \varepsilon_i \cdot \sum_{j=1}^{n} (\varphi_{i \to j} \cdot v_j) \tag{39}$$
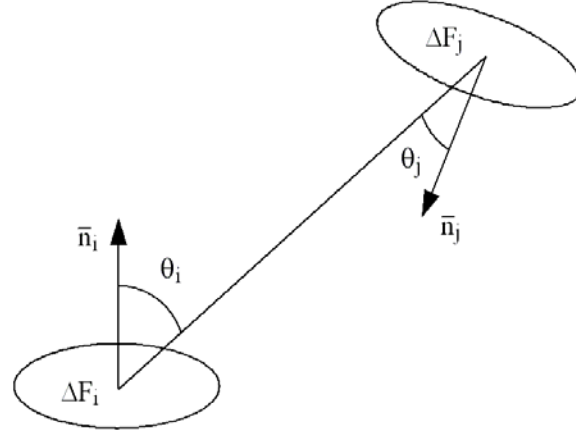
is the adsorbed flux.

Fig. 21: Basis of the view-factor (VF) method

As an example, Fig. 22 shows the comparison of the calculation of the ratio of the pressure at the inlet and outlet of a tube of length $L = 500$ mm and diameter 35 mm, obtained by applying two different methods: the CpoGF method and the VF method.
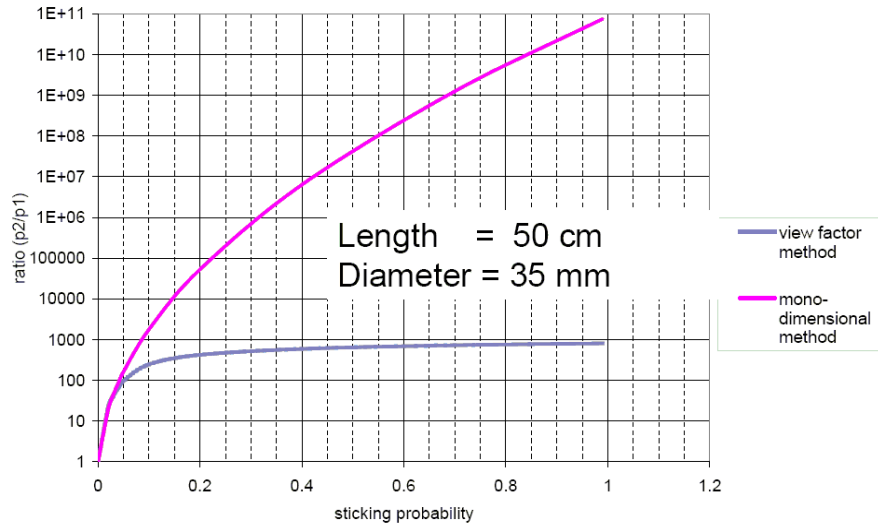

Fig. 22: Comparison between a uni-dimensional analytic method and the VF method [35]

The VF method gives the correct answer, the one that matches the measurements, while the CPoGF method greatly overestimates the pressure ratio at the two ends. This is due to the fact that the latter misses the beaming effect of the molecular flow inside the tube. The two methods agree to some extent only when very small values of the sticking coefficient of the wall are valid, of the order of a few per cent [35].

3.8.1   Commercial programs

Figure 22 has been obtained by applying a proprietary code which implements Eqs. (37–39). Other authors have used some commercial programs which implement the finite-element method (FEM), such as ANSYS, in order to integrate the vacuum and the mechanical calculations all within the same working space [35–37]. In this case, the analogy between radiative heat exchange and molecular flow is such that pressure P is equivalent to the radiation temperature T^4, and the gas flow Q to the radiation heat flow q, through the transformations [36]

$$\begin{cases} \dfrac{P}{k}\sqrt{\dfrac{R}{2\pi MT}} \Leftarrow \sigma T^4 \\ \\ Q \Leftarrow q \end{cases} .$$

(40)

A pump is simulated by transforming the pumping speed S of a pump of area A_p into the 'emissivity' ε_p of the surface simulating the pump

$$\frac{S}{A_p}\sqrt{\frac{R}{2\pi MT}} \Leftarrow \varepsilon_p .$$

(41)

The gas conductance in l/s has its counterpart in the thermal conductance in W/°C.

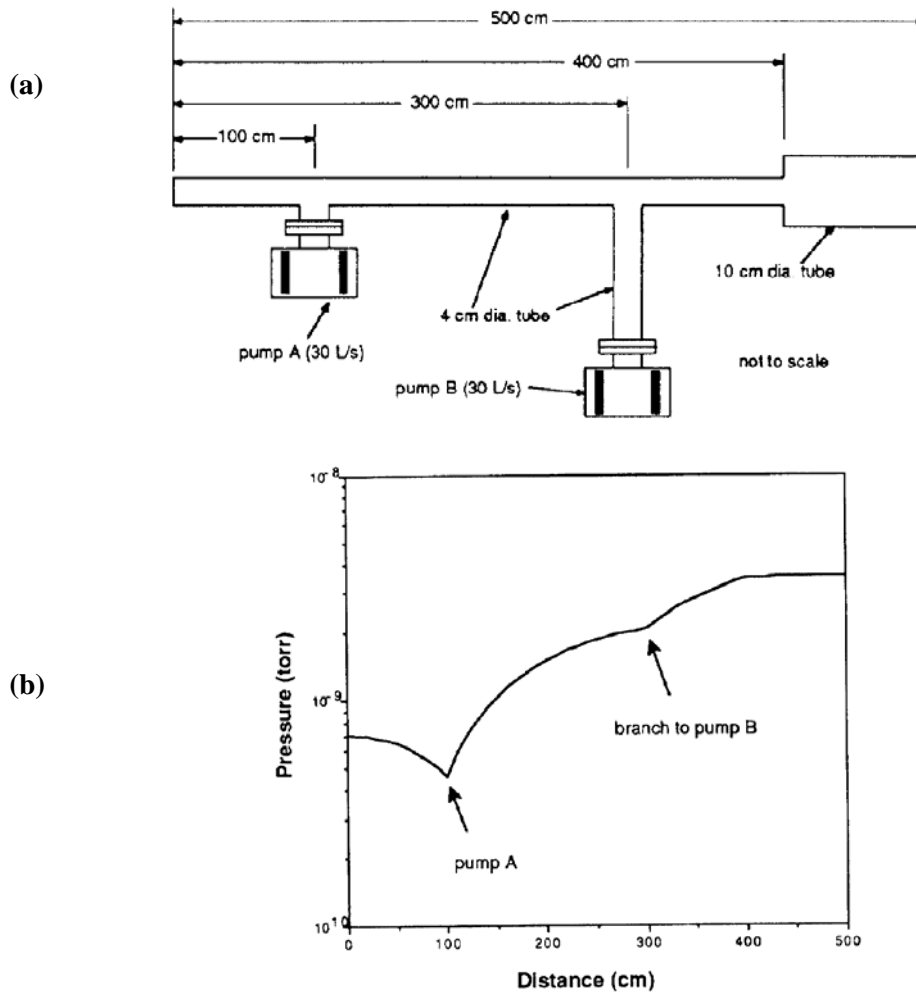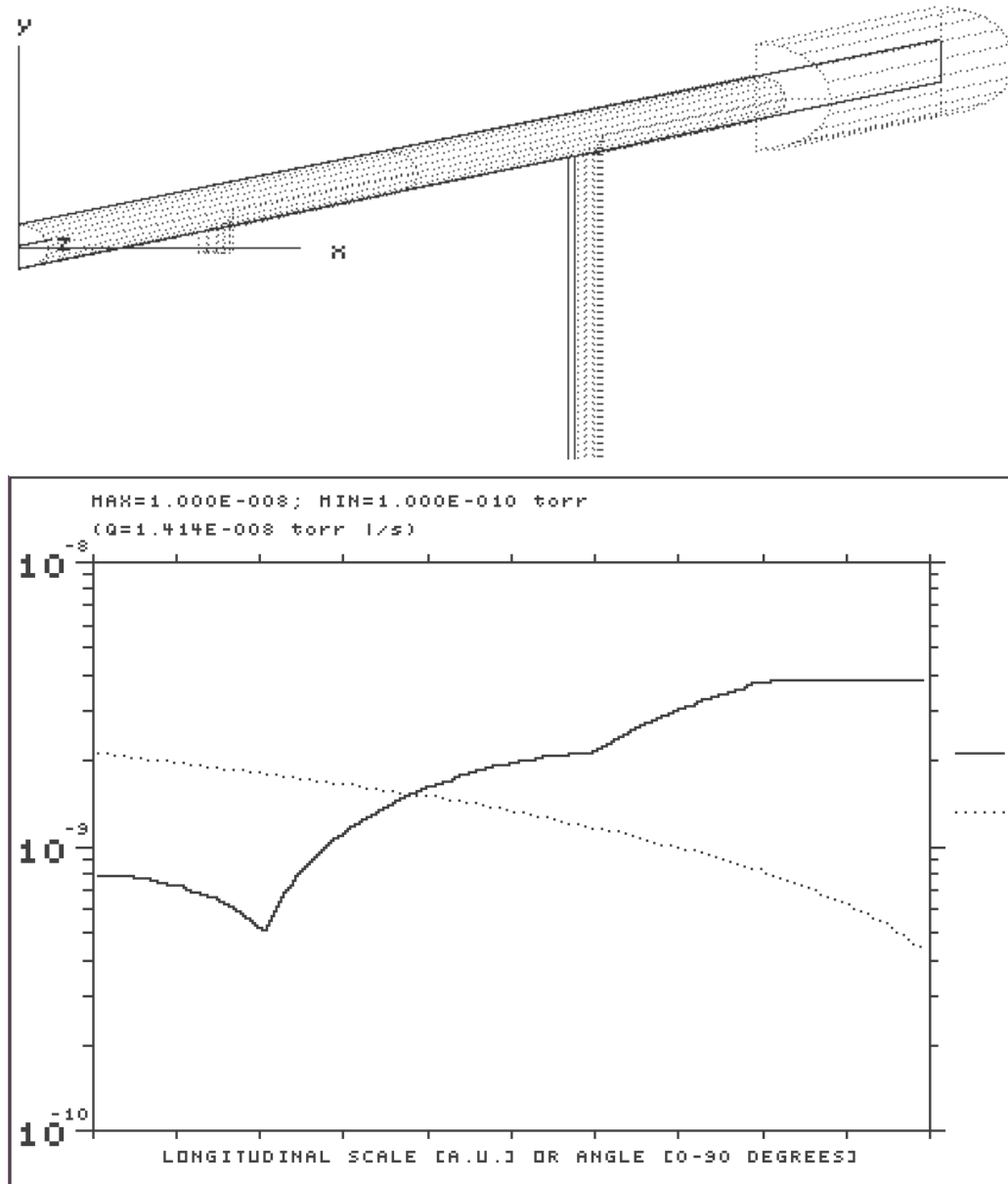**Fig. 23:** (a) Geometry of the vacuum system; (b) Pressure profile calculated with ANSYS [37]

307

MAX=1.000E-008; MIN=1.000E-010 torr
(Q=1.414E-008 torr l/s)

LONGITUDINAL SCALE [A.U.] OR ANGLE [0-90 DEGREES]

Fig. 24: Molflow model of the vacuum system of Fig. 23. Only ½ of the system has been modelled, using the mirror symmetry along the *YZ* plane. The molecules hitting this plane are mirror reflected rather than being reflected diffusively [10]; Pressure profiles calculated with Molflow: solid line = along the 500 cm long tubes; dotted line = along the 100 cm long vertical branch.

Figure 23 shows an example taken from Ref. [37] where the pressure profile along two circular tubes of different diameter connected in series, with a 'tee' along one of the two and two ion-pumps has been calculated using ANSYS. For comparison, Fig. 24 shows a DSMC calculation done with Molflow on the same system.

3.9   Specific conductance calculation

After reviewing many of the different ways to calculate vacuum pressures and other relevant quantities, we come back to the subject of the calculation of the specific conductance of the vacuum chamber of particle accelerators. As mentioned before, the choice of the cross-section of the vacuum chamber is a very important parameter, which could affect the dimension and field quality of the

magnets, the physical aperture of the beam, the beam lifetime, and so on. We have seen that analytic formulae have been developed, together with numerical methods. We propose here to bridge the two fields, by proposing to determine the specific conductance c by using a DSMC calculation and relating it to one analytical model of the pressure profile, the parabolic pressure profile. Let us consider a tube of constant cross-section, with uniform outgassing rate from the walls, pumped at the two ends by two equal pumps. The DSMC model will transform the pumping speeds at the ends into sticking coefficients, as per Eq. (12). The pressure profile obtained by the DSMC method will look like a parabolic one, with a maximum in the middle, and minima at either end, as indicated by Eq. (18). A second-order polynomial fit of the pressure profile will be of the type

$$P'(x) = A_1 x^2 + A_2 x + A_3 \quad . \tag{42}$$

Therefore,

$$
\begin{cases}
A_1 = -\dfrac{Aq}{2c} \\[2mm]
A_2 = \dfrac{AqL}{2c} \\[2mm]
A_3 = \dfrac{AqL}{S}
\end{cases}
\rightarrow
\begin{cases}
c' = \left| \dfrac{Aq}{2A_1} \right| \\[2mm]
c'' = \dfrac{AqL}{2A_2} \\[2mm]
S' = \dfrac{AqL}{A_3}
\end{cases} , \tag{43}
$$

where c', c'', and S' are fitted estimates of c and S.

The following example will show how, for the same cross-sections, estimates of c varying by more than 25% can be obtained, depending on the choice of the method. Figure 25 (a) shows the cross-section of a chamber (pseudo-elliptical part) with an antechamber, similar to what has been used for the Advanced Photon Source synchrotron radiation light source [10]. It is approximately 28 cm in width, and 100 cm long, with a narrow slot of 1 cm height and 12.5 cm width. Molflow has been used to perform two DSMC calculations of the system.

- The first one to calculate the transmission probability, i.e., molecules are generated at the entrance on the plane $Z = 0$ and tracked till the exit at $Z = 100$ cm. Both the entrance and exit facets have a unitary sticking coefficient.

- The second one to calculate the pressure profile when all the side-walls are uniformly desorbing. In this case the pressure profile turns out to be parabolic, and it can be fitted to a second-order polynomial. In this case the 'test facet' which keeps record of all molecular hits used to make up the pressure profile can be chosen in different ways. In this case there are four different types: 1) along the beam chamber (points 43–46); 2) along the antechamber (points 39–42); 3) along the slot (not shown, it lies between the first two); 4) across, i.e., over the whole width of the chamber (i.e., the rectangle identified by points 43, 44, 41, 42). Case no. 3 is a sort of average across the chamber.

The calculation has also been performed using Knudsen's Eq. (2).

Note the large discrepancy between the value of c obtained by the transmission probability and parabolic fit methods, although they are both based on the same DSMC code. This should come as no surprise, as the former assumes molecular effusion (i.e., $\cos\theta$-like with respect to the axis parallel to Z) and therefore there is a non-negligible probability for molecules of travelling straight through the 1 m long chamber, while the latter assumed $\cos\theta$ desorption from the walls, i.e., perpendicular to the longitudinal Z axis of the chamber.

In light of this result, it is suggested to use the DSMC method with a parabolic fit to the pressure profile curve.
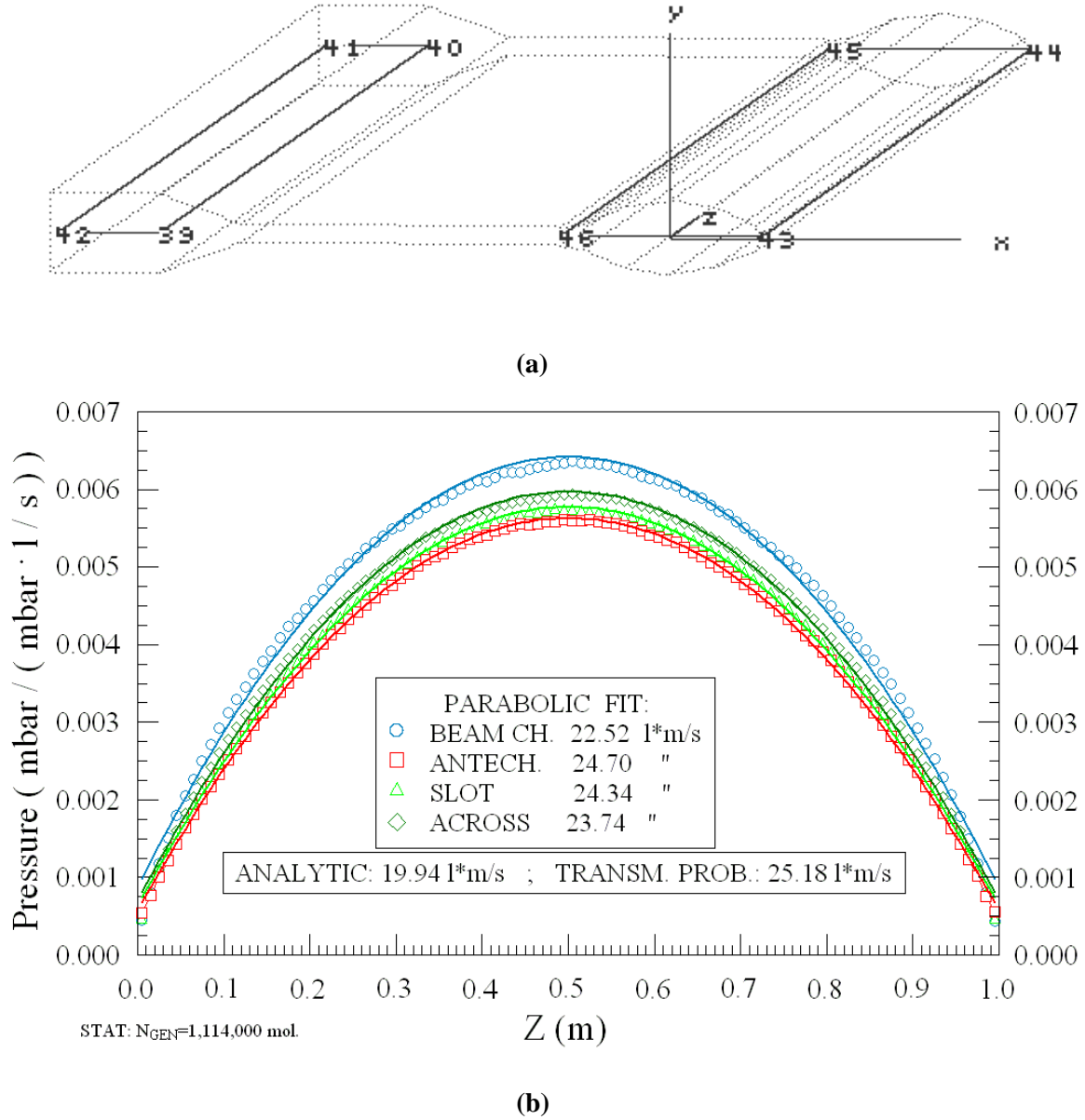

(a)

(b)

Fig. 25: (a) Molflow model of the chamber; (b) Parabolic pressure profiles calculated with Molflow. Note the large discrepancy between the value of *c* obtained by the transmission probability and parabolic fit methods, although they are both based on the same DSMC code.

4   Realistic gas compositions

In the previous sections, we have always made the implicit assumption that there was only one gas species inside the vacuum system. As is well known, this is never the case. Under UHV conditions, it is possible to assume, to a good degree of accuracy, that the total pressure is the sum of the partial pressures [19, 32, 33], which can be calculated as shown before. It is basically Eq. (6) which tells us how the various quantities of interest—pressure, conductance, molecular density and so on—will

310

change. Lighter gas species will have a higher conductance, all other parameters being the same, as will hotter gas species, through the $\sqrt{T/M}$ relationship.

5   Conclusions

In the previous sections, it has been shown that the recent literature is full of examples of pressure calculations performed by using a number of codes and methods, both analytical and numerical. It is left to the reader to make the appropriate choice for the calculation of pressure profiles and related vacuum quantities.

Many examples have been given, trying to point out the strengths and the weaknesses of each method.

Suggestions have been given about the rational choice for the calculation of the specific conductance of the vacuum chamber of particle accelerators.

Acknowledgements

References

[1]   M. Knudsen, Ann. Phys. (Leipzig) [4] **28** (1909) 999–1016.

[2]   P. Clausing, Ann. Phys. (Leipzig) [5] **12** (1932) 961, reprinted in J. Vac Sci. Technol. 8 (1971) 636–646.

[3]   M. Smoluchovski, Ann. Phys. (Leipzig) [4] **33** (1910) 1559.

[4]   W. Steckelmacher, Rep. Prog. Phys. **49** (1986) 1083–1107.

[5]   J.M. Lafferty (ed.), *Foundations of Vacuum Science and Technology* (John Wiley & Sons, New York, 1998).

[6]   B. Dayton, J. Vac. Sci. Technol. **9** (1972) 243–245.

[7]   D.H. Davis, J. Appl. Phys. **31** (1960) 1169.

[8]   C. G. Smith, G. Lewin, J. Vac. Sci. Technol. **3** (1965) 92.

[9]   G. L. Saksaganski, *Molecular Flow in Complex Vacuum Systems* (Gordon and Breach, New York, 1988).

[10]   R. Kersevan, Molflow User's Guide, Sincrotrone Trieste Tech. Note ST/M-91/17, 1991.

[11]   A. Pace and A. Poncet, Monte Carlo simulations of molecular gas flow: some applications in accelerator vacuum technology using a versatile personal computer program, Proc. IVC-11, Cologne, 1989.

[12]   T. Xu, J. M. Laurent and O. Groebner, Monte Carlo simulation of the pressure and the effective pumping speed in the LEP collider, CERN Note CERN-LEP-VA/86-02.

[13]   J. Greenwood, Vacuum **67** (2002) 217–222.

[14]   J. Gomez-Goni *et al*., Vacuum **76** (2004) 83–88.

[15]   J. Gomez-Goni *et al*., J. Vac. Sci. Technol. A **21** (2003) 1452–1457.

[16]   O. Malyshev, Calculation of Gas Flow Through Complex Vacuum Systems, IOP Seminar, London, October 2005.

[17]   K. Brown *et al*., TRANSPORT Manual, SLAC-91, 1977.

[18] V. Ziemann, SLAC-PUB-5962, October 1992.

[19] J. Kurdal, Proc. 45th IUVSTA Workshop on NEG Coatings, Catania, Italy, April 2006.

[20] M. K. Sullivan, A method for calculating pressure profiles in vacuum pipes, SLAC Note, 1993.

[21] K. Gounder *et al*., Residual gas pressure profile in the recycler ring, Proc. PAC 2003, Portland, USA.

[22] Y. Li *et al*., Calculation of pressure profiles in the CESR hardbend and IR regions, Proc. Int. Workshop on Performance and Improvement of e^-e^+ Collider Particle Factories, Tsukuba, 1999.

[23] P. Ladd, SNS, private communication.

[24] R. Kersevan, presentation slides, downloadable at CAS web site: http://cas.web.cern.ch/cas/Spain-2006/Spain-lectures.htm

[25] G. B. Bowden, RF accelerator pressure profile, Linear Collider Collaboration Tech. Note LCC-078, Stanford, 2002.

[26] F.T. Degasperi *et al*, Proc. PAC 2001, Chicago, USA.

[27] B. Plan *et al*., Blue Book, ESRF Note, 2003.

[28] G. K. Green, Spectra and optics of synchrotron radiation, Note BNL 50522, 1976.

[29] D. H. Davis *et al*., J. Appl. Phys. **35** (1964) 529–532.

[30] Y. Suetsugu, J. Vac. Sci. Technol. A **14** (1996) 245–250.

[31] W. C. Turner, Proc. PAC 1993, Washington D.C., USA.

[32] A. Rossi, VASCO: multi-gas code to calculate gas density profile in a UHV system, unpublished CERN note, private communication.

[33] C. Baumgarten *et al*., Eur. Phys. J. **D18** (2002) 37–49.

[34] F. Sharipov *et al*., J. Vac. Sci. Technol. A **20** (2002) 814–822.

[35] A. Bonucci, In-situ characterization of NEG pipe coatings: the transmission factor method, Proc. 45th IUVSTA Workshop on NEG Coatings, Catania, Italy, April 2006.

[36] M. Lafontaine *et al.*, Modeling photoresist outgassing pressure distribution using a finite-element method, ANSYS Conference, 2002.

[37] J. Howell *et al*., Proc. PAC 1991, p. 2297.